arXiv:astro-ph/0503116v2 17 Mar 2005

Constraints on $z \approx 10$ Galaxies from the Deepest HST NICMOS Fields

R.J. Bouwens[2], G.D. Illingworth[2], R.I. Thompson[3], M. Franx[4]

1 Based on observations made with the NASA/ESA Hubble Space Telescope, which is operated by the Association of Universities for Research in Astronomy, Inc., under NASA contract NAS 5-26555.

2 Astronomy Department, University of California, Santa Cruz, CA 95064

3 Steward Observatory, University of Arizona, Tucson, AZ 85721.

4 Leiden Observatory, Postbus 9513, 2300 RA Leiden, Netherlands.

ABSTRACT

We use all available fields with deep NICMOS imaging to search for J_{110}-dropouts ($H_{160,AB} \lesssim 28$) at $z \approx 10$. Our primary data set for this search were the two $J_{110}+H_{160}$ NICMOS parallel fields taken with the Advanced Camera for Surveys (ACS) Hubble Ultra Deep Field (HUDF). The 5σ limiting magnitudes were 28.6 in J_{110} and 28.5 in H_{160} ($0.6''$ apertures). Several shallower fields were also used: $J_{110}+H_{160}$ NICMOS frames available over the Hubble Deep Field (HDF) North, the HDF South NICMOS parallel, and the ACS HUDF (with 5σ limiting magnitudes in J_{110} and H_{160} ranging from 27.0 to 28.2). The primary selection criterion was $(J_{110}-H_{160})_{AB} > 1.8$. Eleven such sources were found in all search fields using this criterion. Eight of these were clearly ruled out as credible $z \approx 10$ sources, either as a result of detections ($> 2\sigma$) blueward of J_{110} or their colors redward of the break ($H_{160}-K \sim 1.5$) (redder than $\gtrsim$98% of lower redshift dropouts). The nature of the 3 remaining sources could not be determined from the data. The number appears consistent with the expected contamination from low-redshift interlopers. Analysis of the stacked images for the 3 candidates also suggests some contamination. Regardless of their true redshifts, the actual number of $z \approx 10$ sources must be ≤ 3. To assess the significance of these results, two lower redshift samples (a $z \sim 3.8$ B-dropout and $z \sim 6$ i-dropout sample) were projected to $z \sim 8-12$ using a $(1+z)^{-1}$ size scaling (for fixed luminosity). They were added to the image frames, and the selection repeated, giving 15.6 and 4.8 J_{110}-dropouts, respectively. This suggests that to the limit of this probe ($\approx 0.3L^*_{z=3}$) there has been evolution from $z \sim 3.8$ and possibly from $z \sim 6$. This

is consistent with the strong evolution already noted at $z \sim 6$ and $z \sim 7.5$ relative to $z \sim 3-4$. Even assuming that 3 sources from this probe are at $z \approx 10$, the rest-frame continuum UV ($\sim 1500\AA$) luminosity density at $z \sim 10$ (integrated down to $0.3L^*_{z=3}$) is just $0.19^{+0.13}_{-0.09}\times$ that at $z \sim 3.8$ (or $0.19^{+0.15}_{-0.10}\times$ including the small effect from cosmic variance). However, if none of our sources is at $z \approx 10$, this ratio has a 1σ upper limit of 0.07.

Subject headings: galaxies: evolution — galaxies: high-redshift

1. Introduction

The detection of galaxies at the highest redshifts ($z \gtrsim 7$) continues to be a difficult endeavor. Due to the redshifting of UV light into the infrared (IR) and the well-known limitations of current IR instruments, searches for these objects require almost prohibitive amounts of telescope time. Nevertheless, small amounts of deep IR data do exist, and they can be used to set constraints on very high redshift galaxies. One notable example is the z_{850}-dropout sample compiled by Bouwens et al. (2004c) which, although limited by small numbers (~ 5 objects) and field-to-field variations, provided a first detection of galaxies at redshifts beyond $z \sim 7$. In this paper, we look at the prevalence of galaxies at $z \sim 8-12$ by applying the dropout technique to the wide variety of deep F110W and F160W-band fields that have been imaged with NICMOS (hereinafter, refered to as J_{110} and H_{160}, respectively). Our principal data set in this study will be the two deep NICMOS parallels taken with the UDF (each has ~ 200 orbits of data), but we will complement this field with a variety of shallower fields possessing similar $J_{110} + H_{160}$ imaging. These fields include the HDF-North Thompson field (Thompson et al. 1999), the HDF-North Dickinson field (Dickinson et al. 1999), the deep HDF-South parallel NICMOS field (Williams et al. 2000), and the NICMOS footprint on the UDF itself (Thompson et al. 2005). Galaxies in the redshift range $z \sim 8-12$ are currently of great interest due to indications that reionization of the universe may have started as soon as $z \sim 17 \pm 5$ (Kogut et al. 2003) and that galaxies may have played a major role in this process (e.g., Yan & Windhorst 2004; Stiavelli et al. 2004). We take $L^*_{z=3}$ to denote the characteristic luminosity of galaxies at $z = 3$ (Steidel et al. 1999). AB magnitudes are used throughout. We assume $(\Omega_M, \Omega_\Lambda, h) = (0.3, 0.7, 0.7)$ (Bennett al. 2003).

2. Observations

(a) NICMOS parallels to the UDF. The two NICMOS parallels to the UDF (taken during the first and second epochs of ACS observations) make up our primary data set. Each parallel consisted of ∼200 orbits of data, split between two pointings which overlap by ∼25% of a NIC3 pointing (∼ 3.0×10^5 s were taken at the first and ∼ 8.6×10^4 s at the second). The observing time at each position was split nearly equally between J_{110} and H_{160}-band observations. While reductions of these fields are available through STScI (http://archive.stsci.edu/prepds/udf/udf_hlsp.html), we used the NICMOS procedures described in Thompson et al. (2005) to perform our own reduction. The deeper of the two pointings making up each parallel had approximate 5σ depths of 28.6 and 28.5 ($0.6''$ aperture) in the J_{110} and H_{160}-bands, respectively. The shallower pointings were some ∼0.6 mags less deep. Our reductions were drizzled onto a $0.09''$-pixel scale, with approximate PSFs of $0.32''$ and $0.34''$ FWHM in the J_{110} and H_{160}-bands, respectively. For optical coverage on these fields, the V_{606} and z_{850}-band images from Galaxy Evolution Morphology Survey (Rix et al. 2004: images #25, #42, and #49) were used (Blakeslee et al. 2003).

(b) Shallower NICMOS Fields. To add area at brighter magnitudes, we included a number of other fields with deep $J_{110} + H_{160}$ imaging in our J_{110}-dropout search. A list of these fields is provided in Table 1, together with their approximate 5σ limiting magnitudes ($0.6''$ aperture) and selection areas. Other multi-wavelength data for these fields include deep $UBVI$ coverage for the HDF-N (Williams et al. 1996), ultra deep ACS $BViz$ coverage for the UDF (Beckwith et al. 2005, in preparation), NICMOS K_{222} coverage of the HDF-S NICMOS parallel (Williams et al. 2000), and deep IRAC data in the 3.6μm and 4.5μm channels for the GOODS North and South (Dickinson et al. 2005, in preparation).

3. Analysis

SExtractor (Bertin & Arnouts 1996) was used to do object detection and photometry. Detection was performed using an aggressive 2σ detection threshold on the H_{160}-band images. Our catalogs were then cleaned of contamination from more extended background artifacts by requiring objects to be 5σ detections in a $0.5''$-aperture. We used scaled aperture magnitudes (Kron 1980: SExtractor MAG_AUTO) for our H_{160}-band total magnitudes. Colors were also measured with scaled apertures, but with a much smaller Kron factor to maximize the S/N. For images with different PSFs, colors were only measured after the higher resolution image had been degraded to match the broader PSF and only in a circular aperture which was at least 2× the FWHM of the broader PSF (see Bouwens et al. 2003 and B05 for more details).

(a) J_{110}-dropout selection. Our principal selection criterion for our sample was a $(J_{110} - H_{160})_{AB} > 1.8$) color cut, where the J_{110}-band flux was replaced by its 1σ upper limit in cases of a J_{110}-band non-detection. This criterion was chosen to minimize contamination from all objects except $z \sim 2-5$ evolved galaxies (Figure 1). In addition, objects were required to be non-detections ($< 2\sigma$) in all optical bands as a result of absorption from the intergalactic medium and to be blue ($\lesssim 1$ mag) in all $H_{160} - K$ or $H_{160} - IRAC$ colors, since only a small fraction ($\lesssim 2\%$) of star-forming galaxies have sufficiently red UV continuum slopes β (i.e., $\beta \gtrsim 0.5$) to produce these colors (Adelberger & Steidel 2000; Schiminovich et al. 2004).

Applying our $(J_{110} - H_{160})_{AB} > 1.8$ color cut to object catalogs from both our primary and shallow search fields, 11 objects were found (Table 2). Of the 11, 6 were readily detected ($> 2\sigma$) in the bluer optical bands. Two had very red $H_{160} - K$ colors (~ 1.5) and so also appear to be low-redshift interlopers. This was a little uncertain for one of the two (HDFSPAR-48278437) due to the marginal nature of its K_{222}-band detection, but IRAC imaging should clarify this issue. The final three sources (shown in Figure 2 with two red objects from our selection) could not be excluded by either criterion, though this may be largely due to the fact they were in the UDF-parallel fields. The optical imaging in these fields are not particularly deep, nor is there any deep Spitzer or K-band data to measure colors longward of the break.

(b) Low-Redshift Contamination. To help determine whether the 3 potential $z \approx 10$ candidates were low-redshift interlopers or not, we made simple estimates of the contamination from different types of sources. The only known stellar sources red enough to match these objects are extreme carbon stars or Mira variables (Whitelock et al. 1995) but contamination from such sources seem unlikely due to both their rarety and high intrinsic luminosities, which would put them well outside the Galaxy (Dickinson et al. 2000). Contamination from redder, evolved galaxies is difficult to estimate given the large uncertainties on the shape of the LF of these galaxies at $z \sim 2-3$. Here, we ignore these complications and simply scatter the colors of a brighter set of galaxies ($H_{160,AB} \sim 24-26$) from our fields to fainter magnitudes. Performing these experiments on the faint source population from the deep parallels, we estimate $\sim 1-3$ such contaminants. This seems consistent albeit a little less than the ~ 3 sources obtained. A stack of the V_{606} and J_{110} exposures for all 3 sources showed detections of 0.8σ and 1.2σ, respectively, again suggesting some contamination.

(c) Expected Numbers/Incompleteness. Having found at most 3 possible $z \approx 10$ sources over our entire 14.7 arcmin^{-2} search area, it is interesting to ask how many we might have expected assuming no-evolution from lower redshift. Two different redshift samples are considered as baselines: (1) a $z \sim 3.8$ B-dropout sample from GOODS (B05) and (2) a $z \sim 6$ i-dropout sample from the HUDF (Bouwens et al. 2005b). As in other recent work (Bouwens

et al. 2004a,b,c), we project this sample to higher redshift (over the range $z \sim 7-13$: see Figure 3) using our well-established cloning machinery (Bouwens et al. 1998a,b; Bouwens et al. 2003; B05), accounting for pixel morphologies, the angular-size distance relationship, NICMOS PSFs, k-corrections, and object-by-object volume densities. Transformed objects are added to the present NICMOS data and the selection procedure repeated. Direct use of the data appears to be the best way of accounting for the substantial variations in S/N which occur across NICMOS mosaics while including possible blending with foreground galaxies. Simulations were run over $\sim$30$\times$ the area of the fields. Assuming no-evolution in size, 5.7 and 4.1 objects are expected in total (over the 6 fields) for our $z \sim 3.8$ B and $z \sim 6$ i-dropout samples, respectively. If we account for the increase in surface brightness expected due to the $\sim (1+z)^{-1}$ size scaling observed at $2 < z < 6$ (Bouwens et al. 2004a,b; Ferguson et al. 2004), the expectations increase to 15.6 and 4.8, respectively. Steeper size scalings (e.g., $(1+z)^{-2}$) yield 21.2 and 6.3 J_{110}-dropouts, respectively, while use of a bluer UV continuum slope β (e.g., $\beta \sim -2.4$) resulted in 16.2 and 4.0, respectively (assuming a $(1+z)^{-1}$ size scaling). We note that the two NICMOS parallels to the UDF account for $\sim$ 73% of the expected numbers (and are therefore our primary constraints), though each of the 6 fields contributes at least a few percent. We take the $(1+z)^{-1}$ scaling estimates, 15.6 from $z \sim 3.8$ and 4.8 from $z \sim 6$ as the most likely expected values.

(d) Previous Work. One previous study of $z \gtrsim 8$ candidates was carried out by Yahata et al. (2001) on the 0.8 arcmin^2 NIC3 parallel to the HDF South featured here. In that paper, 8 $z \gtrsim 10$ candidates were reported (5 of which were selected in the H_{160}-band) based upon 9-band (UBVRIJHK+STIS) photometric redshifts. What became of these 5 candidates here? Looking through our catalogs for this field, we found that one (SB-NI-0915-0620) had $J_{110} - H_{160}$ colors (~ 0.4) that were clearly inconsistent with a high redshift identification. The other 4 appeared to be too faint ($H_{160,AB} \gtrsim 27.5$) to set strong lower limits on the $(J_{110} - H_{160})_{AB}$ colors and thus make robust statements about their redshifts.

4. Implications

We have carried out a search for $z \approx 10$ J-dropouts and found at most 3 possible candidates. Since 15.6 ± 3.9 and 4.8 ± 2.2 candidates are expected (Poisson errors) based on a $(1+z)^{-1}$ scaling of $z \sim 3.8$ and $z \sim 6$ samples, this suggests there has been appreciable evolution at the bright end of the luminosity function. Since an $L^*_{z=3}$ galaxy at $z \sim 10$ has a $H_{160,AB}$-band magnitude of 26.7, our search ($H_{160,AB} \lesssim 28$) tells us something about the galaxy luminosities brightward of $0.3L^*_{z=3}$. For simple Poissonian statistics and assuming that all 3 sources are at $z \approx 10$, the current findings are inconsistent with no-evolution at

the 99.98% and 71% confidence levels, respectively (equivalent to 3.8σ and 1σ).

Of course, cosmic variance is bound to be important for fields of this size. Assuming a selection window of width $\Delta z = 2.5$, a ΛCDM power spectrum, and a bias of 7–which corresponds to the rough volume density of sources $\sim 10^{-4}$ Mpc^{-3} explored by this probe (Mo & White 1996)–we calculate $\sim$27% RMS variations field-to-field for single 0.8 arcmin^2 NIC3 pointings (using a pencil beam window function). Since our deepest two fields provide the primary constraints and they are essentially independent, the total number of J-dropouts found here is expected vary by $\sim$19% RMS relative to the cosmic average. Thus, we expect $\sim 16 \pm 5$ and $\sim 5 \pm 2$ dropouts, respectively, for simple projections of our lower redshift samples, and so the present findings are inconsistent with no-evolution at the 99.9% and 68% confidence levels, respectively (equivalent to 3.3σ and 1.0σ).

It is conventional to cast these findings in terms of the rest-frame continuum UV ($\sim 1500\mathring{A}$) luminosity density. We first estimate the luminosity density under the assumption that the 3 candidates (Figure 2) are at $z \approx 10$. The result is $\rho_{UV}(z \sim 10)/\rho_{UV}(z \sim 3.8) = 0.19^{+0.13}_{-0.09}$ (3 over 15.6 for Poissonian statistics) or $\rho_{UV}(z \sim 10)/\rho_{UV}(z \sim 3.8) = 0.19^{+0.15}_{-0.10}$ (including cosmic variance). Taking the value of the luminosity density at $z \sim 3.8$ (Giavalisco et al. 2004) integrated down to $0.3L^*_{z=3}$, we find a UV luminosity density $\rho_{UV}(z \sim 10) = 2.5^{+1.7}_{-1.2} \times 10^{25}$ erg s^{-1} Hz^{-1} (Poissonian statistics) or $\rho_{UV}(z \sim 10) = 2.5^{+2.0}_{-1.3} \times 10^{25}$ erg s^{-1} Hz^{-1} (including cosmic variance). However, it is quite plausible that none of these candidates are at $z \approx 10$. The expected high contamination level combined with the now well established changes in the LF between $z \sim 6-7$ and $z \sim 3$ suggests that it is more likely that these sources are low redshift objects. Assuming that none are at $z \approx 10$, the 1σ upper limit is: $\rho_{UV}(z \sim 10)/\rho_{UV}(z \sim 3.8) < 0.07$ (both for simple Poissonian statistics and including cosmic variance). In terms of the luminosity density, this limit is $\rho_{UV}(z \sim 10) < 0.9 \times 10^{25}$ erg s^{-1} Hz^{-1}. Adopting a Salpeter IMF and using canonical relations to convert this into a star formation rate density (Madau et al. 1998), we can plot the present determination (integrated down to $0.3L^*_{z=3}$) against previous determinations at lower redshift (Figure 3). The observations now more clearly than before allow us to trace the number of UV-bright systems over the interval $0 < z < 10$. The space density of high luminosity systems seems to peak at $z \sim 2-4$ and decline fairly rapidly to both higher and lower redshift.

As we conclude, it is somewhat sobering to realize that $\sim$740 orbits of deep NICMOS imaging went into this search and only 3 possible $z \approx 10$ candidates were found (all of which may be at low redshift), showing how difficult it is to map out the formation of galaxies at these early times with current technology. It is exciting nevertheless to realize that in the future these surveys will be executed much more efficiently. For example, surpassing the current NICMOS data set would require just $\sim$23 orbits with HST WFC3 and $\sim 1000-2000$

seconds with JWST.

We are grateful to Steve Beckwith and the entire STScI science team for their foresight in taking deep NICMOS parallels to the UDF, Mark Dickinson and STScI for making their NICMOS reductions available in electronic form, Daniel Eisenstein, Bahram Mobasher, and Evan Scannapieco for valuable discussions, Haojing Yan for an electronic copy of a 2.5 Gyr ERO SED, and our referee for valuable comments which substantially improved this manuscript. This research was supported under NASA grant HST-GO09803.05-A and NAG5-7697.

REFERENCES

Adelberger, K. L. & Steidel, C. C. 2000, ApJ, 544, 218.

Bennett, C. L. et al. 2003, ApJ, 583, 1.

Bertin, E. and Arnouts, S. 1996, A&AS, 117, 393.

Blakeslee, J. P., Anderson, K. R., Meurer, G. R., Benítez, N., & Magee, D. 2003, ASP Conf. Ser. 295: Astronomical Data Analysis Software and Systems XII, 12, 257.

Bouwens, R., Broadhurst, T. and Silk, J. 1998a, ApJ, 506, 557.

Bouwens, R., Broadhurst, T. and Silk, J. 1998b, ApJ, 506, 579.

Bouwens, R., Broadhurst, T., & Illingworth, G. 2003, ApJ, 593, 640.

Bouwens, R. J., et al. 2004a, ApJ, 606, L25.

Bouwens, R.J, Illingworth, G.D., Blakeslee, J.P., Broadhurst, T.J., & Franx, M. 2004b, ApJ, 611, L1.

Bouwens, R.J, et al. 2004c, ApJ, 616, L79.

Bouwens, R.J, Broadhurst, T.J., Illingworth, G.D., Meurer, G.R., Blakeslee, J.P., Franx, M., & Ford, H.C. 2005a, ApJ, submitted (B05).

Bouwens, R.J, et al. 2005b, ApJ, in preparation.

Bunker, A. J., Stanway, E. R., Ellis, R. S., & McMahon, R. G. 2004, MNRAS, 355, 374.

Coleman, G. D., Wu, C.-C., & Weedman, D. W. 1980, ApJS, 43, 393.

Dickinson, M. 1999, AIP Conf. Proc. 470: After the Dark Ages: When Galaxies were Young (the Universe at $2 < Z < 5$), 470, 122.

Dickinson, M., et al. 2000, ApJ, 531, 624.

Ferguson, H. C. et al. 2004, ApJ, 600, L107.

Giavalisco, M. et al. 2004, ApJ, 600, L103.

Knapp, G. R., et al. 2004, AJ, 127, 3553.

Kron, R. G. 1980, ApJS, 43, 305.

Madau, P., Pozzetti, L. & Dickinson, M. 1998, ApJ, 498, 106.

Mo, H. J., & White, S. D. M. 1996, MNRAS, 282, 347.

Rix, H., et al. 2004, ApJS, 152, 163.

Schiminovich, D., et al. 2004, ApJ, in press.

Somerville, R. S., Lee, K., Ferguson, H. C., Gardner, J. P., Moustakas, L. A., & Giavalisco, M. 2004, ApJ, 600, L171.

Steidel, C. C., Adelberger, K. L., Giavalisco, M., Dickinson, M. and Pettini, M. 1999, ApJ, 519, 1.

Stiavelli, M., Fall, S. M., & Panagia, N. 2004, ApJ, 610, L1.

Thompson, R. I., Storrie-Lombardi, L. J., Weymann, R. J., Rieke, M. J., Schneider, G., Stobie, E., & Lytle, D. 1999, AJ, 117, 17.

Thompson, R.I., et al. 2005, AJ, submitted.

Whitelock, P., Menzies, J., Feast, M., Catchpole, R., Marang, F., & Carter, B. 1995, MNRAS, 276, 219.

Williams, R.E., et al. 1996, AJ, 112, 1335.

Williams, R. E., et al. 2000, AJ, 120, 2735.

Yahata, N., Lanzetta, K. M., Chen, H., Fernández-Soto, A., Pascarelle, S. M., Yahil, A., & Puetter, R. C. 2000, ApJ, 538, 493.

Yan, H. & Windhorst, R. A. 2004, ApJ, 612, L93.

Yan, H., et al. 2004, ApJ, 616, 63.

This preprint was prepared with the AAS LaTeX macros v5.2.

Table 1. J_{110}-dropout Search Fields.

Field	Area ($\Box'$)	5σ limit J_{110}	H_{160}
HDF-N Thompson	0.8	27.8	28.1
HDF-N Dickinson	5.2	27.2	27.0
HDF-S NIC-Par	0.8	28.2	28.2
UDF NIC-Par-1	1.3	28.6	28.5
UDF NIC-Par-2	1.3	28.6	28.5
UDF Thompson	5.5	27.7	27.5

Table 2. Red $(J_{110} - H_{160})_{AB} > 1.8$ objects in our search fields.[a]

Object ID	R.A.	Decl.	H_{160}	$J-H$	$V-H$	$z-H$	$H-K$	$H-m_{3.6\mu m}$	$r_{hl}('')$
UDF-39188323	03:32:39.18	-27:48:32.3	23.3±0.1	2.0	3.8	2.5	0.4	1.2	0.26
UDF-42888094	03:32:42.88	-27:48:09.5	24.8±0.1	2.7	4.3	3.3	1.0	2.9	0.25
UDFNICPAR1-01191115	03:33:01.23	-27:41:11.5	27.0±0.1	1.8	0.9	>-0.2	—	—	0.24
UDFNICPAR1-04151142	03:33:04.18	-27:41:14.1	28.2±0.2	1.8	>-0.0	>-1.3	—	—	0.18
UDFNICPAR1-05761077	03:33:05.80	-27:41:07.6	27.8±0.2	>2.0	>0.3	>-1.0	—	—	0.21
UDFNICPAR2-07352493	03:33:07.35	-27:52:49.3	27.9±0.2	1.8	0.6	>-0.7	—	—	0.14
UDFNICPAR2-09593048	03:33:09.59	-27:53:04.8	27.3±0.2	1.9	>0.9	>-0.4	—	—	0.19
HDFN-46242594	12:36:46.24	62:12:59.4	26.5±0.1	>2.1	1.1	—	<1.7	—	0.17
HDFN-51763567	12:36:51.76	62:13:56.7	25.0±0.1	2.0	2.1	—	0.6	—	0.31
HDFN-56253227	12:36:56.25	62:13:22.7	25.2±0.1	>3.2	>4.2	—	1.5	2.0	0.20
HDFSPAR-48278437	22:32:48.27	-60:38:43.7	26.0±0.1	>2.5	—	—	1.5	—	0.32

[a]All astrometry uses the J2000 equinox. Magnitudes are in the AB system. All limits are 2σ except the limits on the $J_{110} - H_{160}$ color which are only 1σ. Total magnitudes and colors are derived in Kron apertures of different sizes (B05). Object IDs are the last four significant figures given in this table for the Right Ascension and Declination.

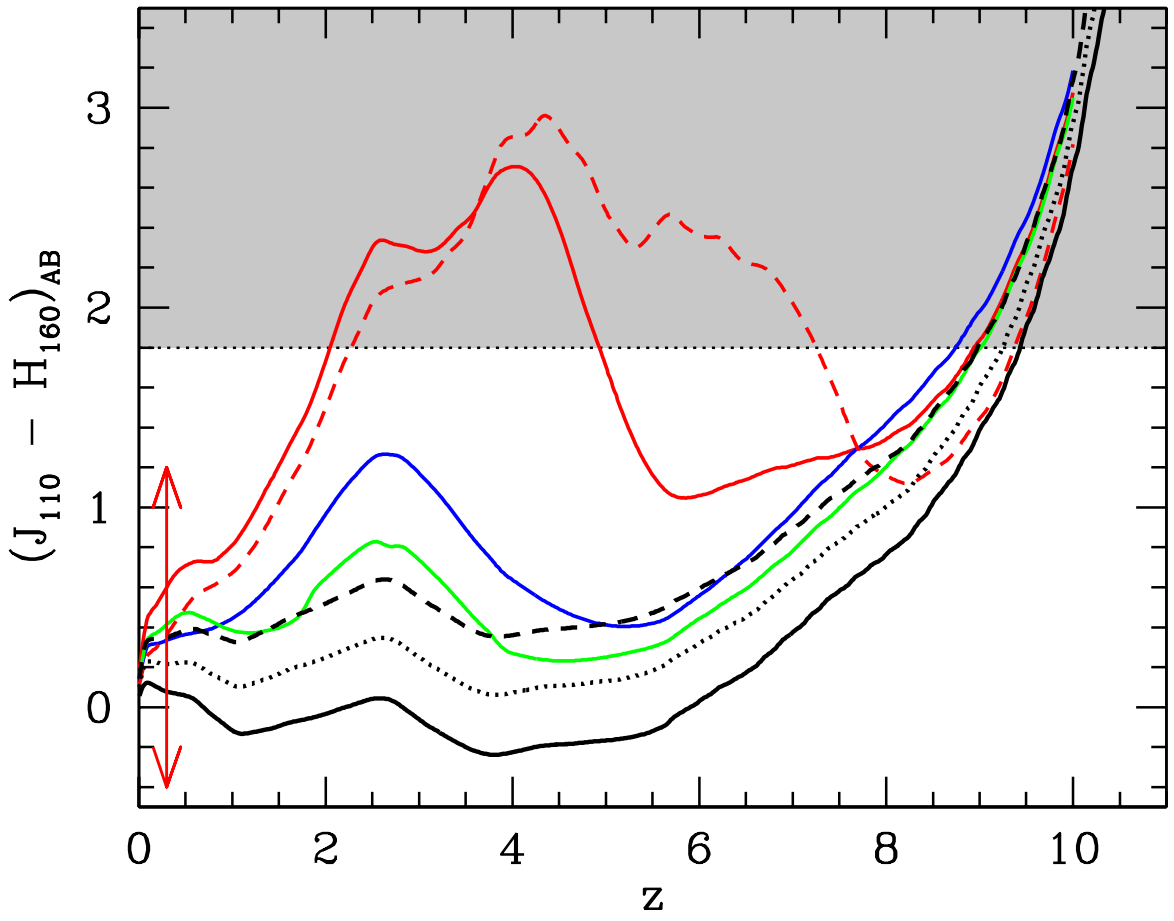

Fig. 1.— $(J_{110} - H_{160})_{AB}$ color versus redshift for a number of different SEDs. Shown are the Coleman, Wu, & Weedman (1980) elliptical template (*red line*), Sbc template (*blue line*), Scd template (*green line*), and different reddenings ($E(B-V) = 0.0, 0.15, 0.3$) applied to a 10^8 yr burst (*black solid, dotted, and dashed lines, respectively*). Extremely red objects such as those found in recent IRAC selections (e.g., Yan et al. 2004) have very similar colors (in the infrared) to 2.5 Gyr bursts and are included here as the dashed red line. The red arrow near $z \sim 0$ denotes the range of colors expected for low mass stars (Knapp et al. 2004). Our $(J_{110} - H_{160})_{AB} > 1.8$ J_{110}-dropout criterion is shown as a dotted horizontal line and provides a good balance between minimal contamination (selecting evolved SEDs at intermediate redshifts $z \sim 2 - 5$) and selecting objects at $z \approx 10$.

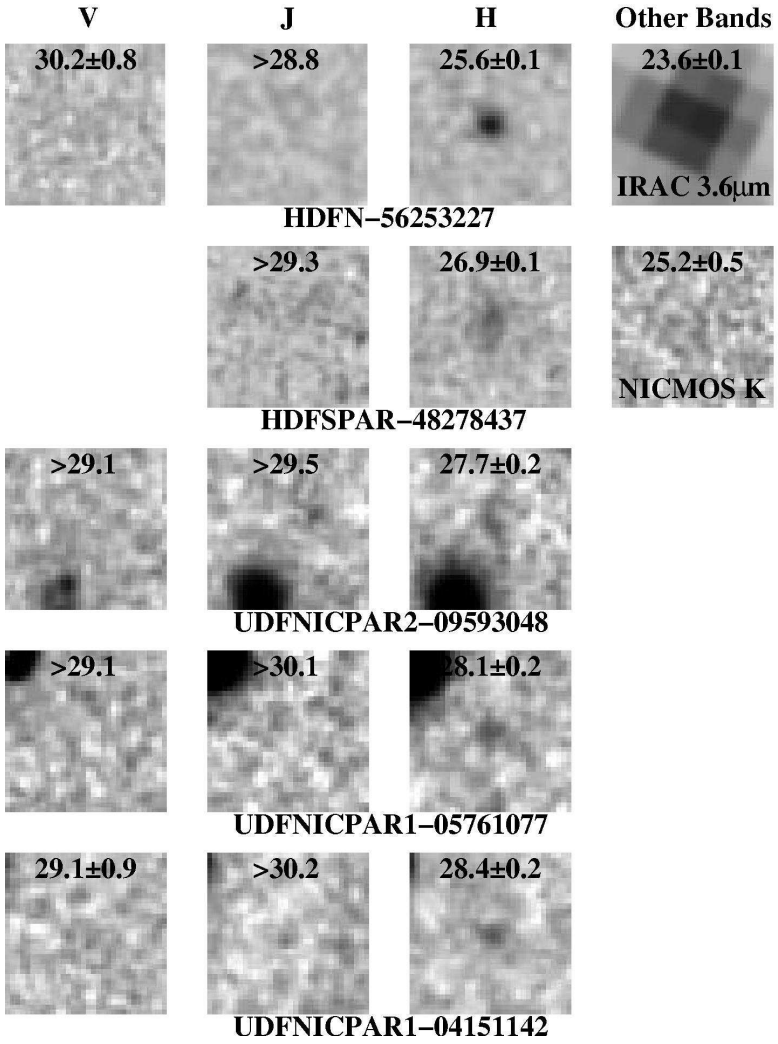

Fig. 2.— Postage stamps images ($J_{110}H_{160}$ bands) of 5 objects which met our $(J_{110} - H_{160})_{AB} > 1.8$ selection. The leftmost and rightmost columns show postage images in a bluer (V_{606} band) and redder band (the IRAC 3.6μm channel for HDFN-56253227 and NICMOS K_{222} for HDFSPAR-48278437), respectively. The overplotted magnitudes (and 1σ upper limits) were measured within a 0.6″-diameter aperture. The object in the top row (HDFN-56253227) is the well-known Dickinson et al. (2000) J_{110}-dropout. Its extremely red colors ($(H_{160} - K)_{AB} = 1.5$ and $(H_{160} - IRAC_{3.6\mu m})_{AB} = 2$) suggest that it is at low redshift ($z \sim 2 - 3$). The second object (HDFSPAR-48278437) was similarly excluded from our list of $z \approx 10$ candidates because of its marginal detection ($\approx 2\sigma$) in the NICMOS K_{222}-band and $(H_{160} - K_{220})_{AB}$ color of 1.5. The final three objects could be at $z \approx 10$, but await limits at longer wavelengths (from Spitzer) and good optical data to exclude the possibility that they are highly reddened or evolved galaxies. Objects UDFNICPAR2-09593048 and UDFNICPAR1-04151142 appear to be just detected in the J_{110}-band at the 1σ level, so this may indicate they are low redshift interlopers. The final object (UDFNICPAR1-04151142) is just marginally resolved, but the only stellar sources red enough to match its colors would appear to be too bright (§3b). Each postage stamp is 2.9″×2.9″ in size.

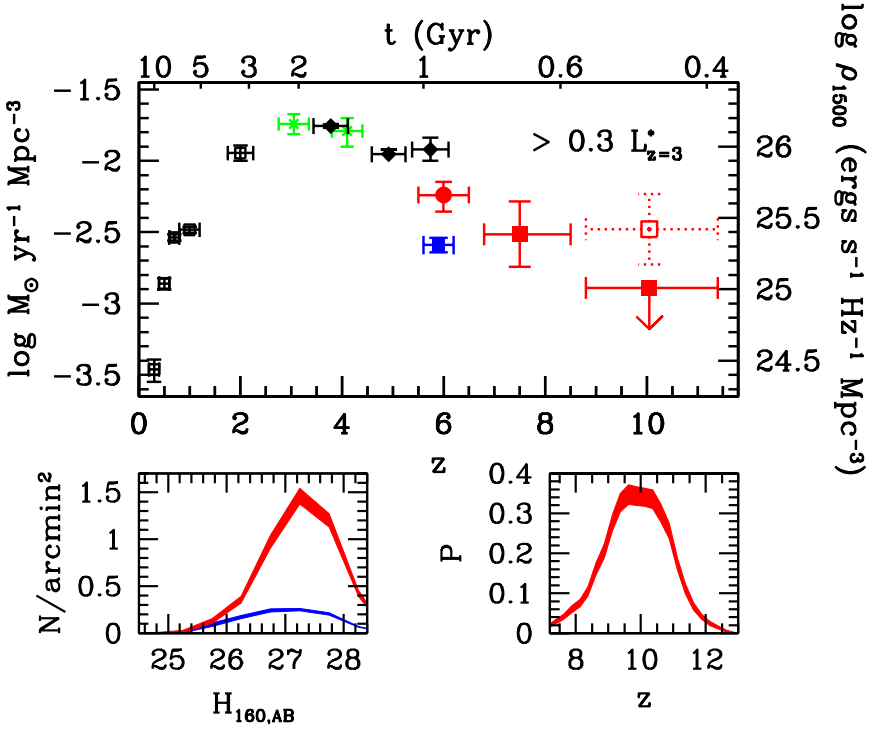

Fig. 3.— The cosmic star formation rate density versus redshift with no extinction correction. The star formation rate density (integrated down to 0.3 $L^*_{z=3}$ – the limit of our $z \sim 10$ search) was calculated from the luminosity density in the rest-frame UV continuum ($\sim 1500\AA$: plotted on the right vertical axis) using canonical assumptions (e.g., Madau et al. 1998) and a Salpeter IMF. The open red square at $z \sim 10$ shows our result if 3 objects from this study prove to be at $z \approx 10$, while the large downward pointing arrow shows our 1σ limits if none are (see text). Included on this plot are also estimates by Schiminovich et al. (2004) (open black squares), Steidel et al. (1999) (green crosses), Giavalisco et al. (2004) (black diamonds), Bunker et al. (2004) (solid blue square), Bouwens et al. (2004c) (solid red square), and Bouwens et al. (2005b) (solid red circle). Consistent with past practice, the error bars reflect poissonian uncertainties. Large scale structure (cosmic variance) would add an estimated $\pm 20\%$ for many of the lower redshift points (e.g., Somerville et al. 2004), $\pm 50\%$ for the $z \sim 7.5$ point, and $\pm 19\%$ for the $z \sim 10$ point. Lower left: The surface density of J_{110}-dropouts predicted from a $(1+z)^{-1}$ size scaling of a $z \sim 3.8$ B-dropout sample from GOODS (B05) at the depths of the NICMOS parallels to the UDF (shaded red regions). The blue shaded regions show the equivalent surface density for all our search fields. The drop in the predicted counts at fainter magnitudes arises from incompleteness. Lower right: The redshift distribution for objects satisfying our J_{110}-dropout criterion in the above simulations (after distributing our "cloned" objects over the interval $z \sim 7 - 13$ in proportion to the cosmological volume element). The primary conclusion to be drawn from these results is